Quasifree $(\vec{d}, {}^2\mathrm{He})$ data

T. Sams, C. Ellegaard, C. Gaarde, and J. S. Larsen
Niels Bohr Institute, Blegdamsvej 17, DK-2100 Ø, Denmark

J. L. Boyard, T. Hennino, J. C. Jourdain, B. Ramstein, and M. Roy-Stephan
Institut de Physique Nucléaire, Institut National de Physique Nucléaire et de Physique des Particules/CNRS and Université de Paris-Sud, F-91406 Orsay Cedex, France

P. Radvanyi
Laboratoire National Saturne, CEA/DSM and Institut National de Physique Nucléaire et de Physique des Particules/CNRS, CEN SACLAY, F-91191 Gif-sur-Yvette, France

A. Brockstedt and M. Österlund
University of Lund, S-22362 Lund, Sweden

P. Zupranski
Institute for Nuclear Studies, Warsaw, Poland

C. D. Goodman
Indiana University, Bloomington, Indiana 47408

M. Ichimura
University of Tokyo, Komaba, Meguro-ku, Tokyo 153, Japan

V. F. Dmitriev
Institute of Nuclear Physics, 630 090 Novosibirsk-90, Russia
(Received 16 November 1994)

Experimental data on the nuclear spin-isospin response in the quasifree region, measured with the charge-exchange reaction $(\vec{d}, 2p\,[^1S_0])$ at Laboratoire National Saturne, are presented. The use of a tensor-polarized beam enables us to separate the tensor analyzing powers T_{20} and T_{22}. The present publication is intended to serve as a compilation of the complete set of quasifree data with the $(\vec{d}, {}^2\mathrm{He})$ reaction at 1.6 GeV bombarding energy. Data for $^{12}\mathrm{C}$ are compared to calculated cross sections and tensor-analyzing powers. The cross section in the high-energy end of the quasielastic peak is underestimated, whereas the polarization observables are reasonably well reproduced. The distortion effects are, however, found to be large, suggesting that the $(\vec{d}, {}^2\mathrm{He})$ reaction is not sensitive to spin correlations in the continuum.

PACS number(s): 25.45.Kk, 24.70.+s, 24.50.+g, 25.40.Kv

I. INTRODUCTION

The present paper is a contribution to the understanding of the response of a nucleus to the pion field in the quasifree region. The reaction used is the charge-exchange spin-transfer reaction $(\vec{d}, 2p\,[^1S_0])$, also called $(\vec{d}, {}^2\mathrm{He})$. This reaction selectively probes the spin-isospin structure of nuclei. At low energy transfer, e.g., bound states and low-lying resonances, the probe provides an appropriate tool to separate the nuclear response in individual spin channels. However, as will become clear in the following, the probe is, unfortunately, and contrary to expectations, to a large extent masked by distortion and not able to separate the individual spin channels of the nuclear response function in the continuum. We present for the first time a complete description of the spin structure of the $(\vec{d}, {}^2\mathrm{He})$ reaction at intermediate energy.

The isospin channel of the nucleon-nucleon interaction is strongly spin dependent.[1] When the momentum transfer is larger than the pion mass, the spin-longitudinal and

[1]The strong spin dependence of the interaction is due to the pseudoscalar nature of the one-pion exchange. The OPE is purely spin longitudinal: the Pauli operator $\boldsymbol{\sigma}$ acting in the spin space of the nucleon acts "along" the momentum transfer $\mathbf{q}$. However, even the large spin-transverse components of the isospin channel are determined by the pion exchange mechanism: they result from a screening of the OPE at small impact parameters. This holds for the two prototype reactions of the isospin channel, the excitation of the Δ (1232 MeV) isobar in $\mathrm{N}+\mathrm{N} \rightarrow \mathrm{N}+\Delta$ and the elementary charge exchange reaction $n+p \rightarrow p+n$ [21,40,41]. This means that the spin-isospin channel of the nuclear response is determined by the structure of the pion-nucleon vertex.

the spin-transverse amplitudes even have opposite signs. Similar contrast between the longitudinal and transverse spin channel was expected in the residual interaction. After Alberico, Ericson, and Molinari pointed out that a random-phase approximation (RPA) calculation of the nuclear response in the continuum leads to a downward shift (softening) of the spin-longitudinal response versus an upward shift (hardening) of the spin-transverse response [1–3], much interest was devoted to this subject, experimentally as well as theoretically.

Only hadronic probes are sensitive to both the spin-longitudinal and the spin-transverse response. Electron scattering is sensitive to the spin-scalar and the spin-transverse nuclear response. (The spin-scalar response is in the electron-scattering community called the longitudinal response.) A recent analysis of electron-scattering data on ^{4}He suggests that part of the contribution from the one-body operator of the probing field is shifted to high excitation energies, leading to an apparent downward shift of the strength in the quasielastic region [4]. This refers then to strength associated with one-particle–one-hole excitations of the correlated ground state and the shift is found for both the spin-scalar and spin-transverse strength. The two-body part of the probing field (e.g., probing meson exchange currents in the nucleus) gives, however, a significant contribution to the spin-transverse cross section, to give a net enhancement of the spin-transverse part.

We note that the corresponding analysis for hadronic probes, i.e., including also two-body operators in the probing field, has not been performed. In the hadron case we furthermore expect contributions from two-step processes on the projectile-target level.

The experimental study of the quasielastic excitation of nuclei with the $(^3\mathrm{He}, t)$ reaction results in a dispersion relation deviating substantially from that on a free nucleon [5]

$$\omega_{\mathrm{lab}} = \frac{\mathbf{q}^2}{2m_N} \,. \tag{1}$$

At large momentum transfers, of order 2–3 times the Fermi momentum, the quasielastic peak is shifted substantially downwards, whereas it qualitatively agrees with the value given by (1) at momentum transfers close to the Fermi momentum. The observed dispersion relation corresponds rather closely to distributing the available momentum transfer on two target nucleons. With the $(d, ^2\mathrm{He})$ probe, as will be shown in the present paper, the same behavior is seen. One major reason for studying the spin-isospin excitation of nuclei in selected spin channels is to determine whether these shifts might be related to a polarization of the nuclear medium. Notably, the (p, p') reaction follows the free dispersion relation, whereas for the (e, e') and (p, n) reactions there is an upward shift by a constant [5–8].

In the $(d, ^2\mathrm{He})$ reaction, the interference between the $^3S_1$ and the $^3D_1$ state in the deuteron projectile gives rise to a preference for spin-longitudinal excitation [9–12]. A similar effect is present in $(^3\mathrm{He}, t)$. In combination with the softening and enhancement of the spin-longitudinal response predicted at momentum transfers $q \sim 1.7\,\mathrm{fm}^{-1}$ in RPA calculations [2,3], this has been thought to be the reason why the shift occurred specifically in charge-exchange reactions with composite probes. In this light it is surprising to observe that the downward shift is accompanied by a very strong enhancement of the spin-transverse cross section in $(\vec{d}, ^2\mathrm{He})$ [13,14].

The prediction of an enhancement of the spin-longitudinal over the spin-transverse response is contradicted by the investigation of the spin-isospin response with the $(\vec{p}, \vec{p}\,')$ experiment [15,16], and more recently in an experiment with the $(\vec{p}, \vec{n})$ probe at LAMPF [8,17–19]. In these experiments a slight suppression of the ratio of spin-longitudinal over spin-transverse cross sections is observed in nuclei at $1.7\,\mathrm{fm}^{-1}$ momentum transfer. The origin of this unexpected strength in the spin-transverse channel is a current issue of debate [20]. We note that the recent model calculations of the one-body operator part of the spin-transverse response do not predict an enhancement.

At Laboratoire National Saturne, we have used the high quality tensor polarized deuteron beam to study the nuclear response with the charge-exchange probe $(\vec{d}, 2p)$. Concerning spin observables, it provides the same rank of information as the $(\vec{p}, \vec{n}\,)$ experiment. In the $(d, 2p\,[^1S_0])$ reaction the isospin transfer in the probe serves to select the isospin channel. Further, the spin transfer in the probe helps to exclude the spin-scalar reaction channel. With this probe, we are thus directly in the spin-isospin channel. With the use of a tensor polarized deuteron beam we obtain data from which spin-longitudinal and spin-transverse cross sections can be extracted. Partial results have previously been reported [13,14,21,22].

Further, we present a detailed calculation taking into account the nuclear distortion on the two probe nucleons separately, and show that distortion effects lead to an enhancement of the transverse over longitudinal cross section in $(d, ^2\mathrm{He})$ as observed at $1.7\,\mathrm{fm}^{-1}$and larger momentum transfers. Further, the same calculation indicates that distortion can explain the observed enhancement of the spin-longitudinal over spin-transverse cross section at $q = 1.3\,\mathrm{fm}^{-1}$.

II. EXPERIMENT

The $(\vec{d}, 2p)$ experiments were performed using the polarized deuteron beam at Laboratoire National Saturne. Since the upgrade with the MIMAS preaccelerator Saturne delivers up to 10^{11} deuterons per burst [23]. The ion source delivers an 85% tensor polarized beam whose polarization remains practically unchanged during the acceleration [24]. This means that the experiment was performed with beam polarization $\rho_{20} = 0.61 \pm 0.01$ quantized along the symmetry axis of the synchrotron, to be compared to a maximal theoretical value of $1/\sqrt{2}$. Further, by precessing the deuteron spin in a superconducting solenoid before the target, it was possible to obtain other beam polarizations. Data were recorded at bombarding energies 1.6 GeV and 2.0 GeV.

In order to minimize background from sequential breakup of two deuterons, the two protons were required

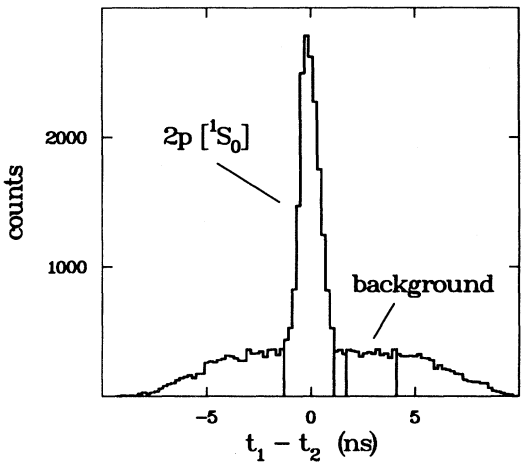

FIG. 1. Spectrum of the measured difference in time of arrival of the two protons at the intermediate focal plane. The true events fall inside the peak representing two protons arriving "simultaneously." Consecutive breakup of two deuterons gives the flat background. This background is minimized, setting a software gate around the peak as indicated. The remaining background can be subtracted by setting a gate of the same size in the flat region and subtracting the events falling in this gate from the events inside the true gate.

to arrive in coincidence ($\sim$ 2 ns time window) in plastic scintillators at the intermediate focal plane 16 m after the target. As shown in Fig. 1, by setting the coincidence window a few ns off, a background spectrum is obtained.

The two protons were detected individually in the spectrometer SPES4 [25]. The cuts from the 1.7°×2.6° collimator and from the spectrometer restrict the relative motion of the $2p$ system to the $^1S_0$ state with high efficiency [26]. This serves to select the spin-transfer channel.

The measured spectrum of the relative momentum of the two detected protons is shown in Fig. 2. Also the calculated distribution, taking into account the cuts from the collimator and from the spectrograph, is shown.

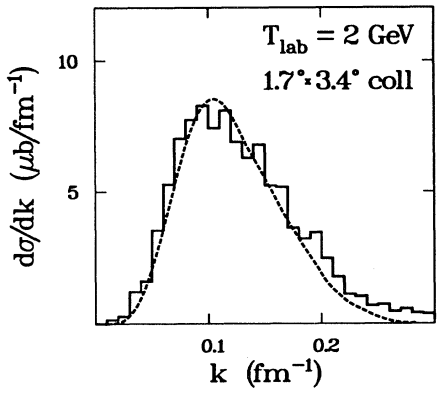

FIG. 2. The distribution of the relative momentum of the two protons of the outgoing unbound ^{2}He at bombarding energy $T_{\rm lab}$ = 2 GeV, 2.3° laboratory scattering angle, and collimator 1.7°×3.4°. The observed spectrum is compared with the calculated taking into account the cuts from the spectrometer and the collimator.

As reference and test targets we have used liquid H_2 and D_2 (100–300 mg/cm^2). The yield from the "empty" target consisting of Ti and Mylar foils (total of 30 mg/cm^2) was subtracted. The nuclear targets for which we have performed the most detailed studies were ^{12}C and ^{40}Ca foils of thicknesses 50–500 mg/cm^2.

The spectrograph was run in a mode where it covers ±3.5% around the central momentum setting. In $(d, 2p)$, however, the efficiency falls off rather fast when the extreme momenta are approached. In order to have sufficient overlap of field settings only the central ±2.5% were used. Spectra covering energy transfers from 0 to 500 MeV could thus be obtained from 7 magnetic field settings each taking typically 30 min. Spectra were recorded at 5 angles allowing us to cover a momentum transfer from 0 to 2.4 fm^{-1}.

III. ANALYSIS

A. Observables

The observables are the differential cross section and the tensor analyzing powers. The normalization of the scattering matrix $\mathcal{M}$ is such that

$$\frac{d^2\sigma}{dt\,d\omega} = \frac{1}{3}\frac{1}{64\pi F^2}\mathrm{tr}(\mathcal{M}\mathcal{M}^\dagger), \tag{2}$$

where $F = (p_1p_2 - m_1m_2)^{\frac{1}{2}} = |\mathbf{p}_{1\,\rm lab}|m_{\rm target}$ is Møller's invariant flux factor. The tensor analyzing powers

$$T_{\lambda\mu} = \frac{\mathrm{tr}(\mathcal{M}\,\tau_{\lambda\mu}\,\mathcal{M}^\dagger)}{\mathrm{tr}(\mathcal{M}\mathcal{M}^\dagger)} \tag{3}$$

refer to the Madison frame, i.e., z axis along the beam and y axis along the normal $\mathbf{p}_1\times\mathbf{p}_3$ to the scattering plane [27]. The operator τ acting in the spin space of the deuteron is normalized as $\langle 1M' \,|\, \tau_{\lambda\mu} \,|\, 1M\rangle = \sqrt{2\lambda+1}\ \langle 1M\,\lambda\mu|1M'\rangle$. The restriction from parity conservation of strong interactions implies the symmetry relation $T_{\lambda\mu} = (-)^{\lambda-\mu}T_{\lambda-\mu}$ for the tensor analyzing powers [28]. This leaves only T_{20}, T_{21}, and T_{22} as independent rank two analyzing powers.

For a beam with spin density

$$\rho = \frac{1}{2s+1}\sum_{\lambda\mu}\rho_{\lambda\mu}\,\tau^\dagger_{\lambda\mu} = \frac{1}{2s+1}\sum_{\lambda\mu}\langle\tau_{\lambda\mu}\rangle\,\tau^\dagger_{\lambda\mu}, \tag{4}$$

the cross section is

$$d\sigma = (d\sigma)_0\sum_{\lambda\mu}\rho_{\lambda\mu}T^\dagger_{\lambda\mu}\ . \tag{5}$$

The polarization of the beam coming out of the synchrotron is along the symmetry axis of the acceleration ring. Precessing the deuteron spin in a superconducting solenoid makes it possible to obtain other directions of

polarizations of the beam on the target. Thus, it has been possible to determine combinations of T_{20}^M and T_{22}^M of the form

$$\frac{d\sigma}{(d\sigma)_0} = \rho_{20}^{\text{beam}}\, T_{20}^{\text{beam}} = \rho_{20}^{\text{beam}} \left\langle \frac{1}{2} T_{20}^M + \sqrt{\frac{3}{2}} \cos 2\varphi\, T_{22}^M \right\rangle \simeq \rho_{20}^{\text{beam}} \left(\frac{1}{2} T_{20}^M + \sqrt{\frac{3}{2}} \langle \cos 2\varphi \rangle\, T_{22}^M \right) . \quad (6)$$

The polarization of the beam, along the internal polarization axis, was $\rho_{20}^{\text{beam}} = 0.61 \pm 0.01$. In the following, the analyzing powers refer to the Madison frame [29]. At finite scattering angles, the angle φ between the normal to the reaction plane and the beam polarization direction could be varied between 0° and 45°.

For readers more familiar with the Cartesian tensor analyzing powers, the transformation goes as

$$A_{xx} = -\sqrt{2} \left(\frac{1}{2} T_{20} - \sqrt{\frac{3}{2}} T_{22} \right) , \quad (7)$$

$$A_{yy} = -\sqrt{2} \left(\frac{1}{2} T_{20} + \sqrt{\frac{3}{2}} T_{22} \right) . \quad (8)$$

B. The $(d, {}^2\text{He})$ form factor

The deuteron wave function consists of a ${}^3S_1$ and a ${}^3D_1$ wave part. The radial wave functions U and W shown in Fig. 3 are taken from the Paris parametrization [30]

$$\psi_d(\mathbf{s}) = \frac{U(s)}{s} Y_{00}(\mathbf{s}) \,|\, (\tfrac{1}{2}\tfrac{1}{2})1M \rangle + \frac{W(s)}{s} \left(Y_2(\mathbf{s}) \,|\, (\tfrac{1}{2}\tfrac{1}{2})1 \rangle \right)_{(2\,1)1M} . \quad (9)$$

The ${}^1S_0$ state of the $2p$ system is described by the wave function

$$\psi_{2p}(\mathbf{s}) = \frac{u_k(s)}{s} Y_{00}(\mathbf{s}) \,|\, (\tfrac{1}{2}\tfrac{1}{2})00 \rangle , \quad (10)$$

where the radial wave function u_k is the regular solution of the Schrödinger equation

$$\left(-\frac{1}{2\mu} \frac{d^2}{ds^2} + V_{\text{Reid}}(s) + \frac{e^2}{s} \right) u_k(s) = \frac{k^2}{2\mu} u_k(s) . \quad (11)$$

V_{Reid} is the Reid soft-core parametrization of the isospin triplet, spin singlet nucleon-nucleon interaction [31]. u_k is normalized to

$$u_k(s) \simeq \frac{\sqrt{4\pi}}{k} \sin[k\,s - \eta \ln(2\,k\,s) + \sigma_0 + \delta] \quad , \quad \text{as } s \to \infty \quad (12)$$

corresponding to the plane wave box normalization $\langle \mathbf{k}' \,|\, \mathbf{k} \rangle = (2\pi)^3\, \delta^{(3)}(\mathbf{k}' - \mathbf{k})$ (μ = reduced mass, $\eta = \mu e^2/k$, σ_0 = Coulomb phase shift, δ = nuclear phase shift [32]).

The $(d, {}^2\text{He})$ form factor, which is calculated in the probe Breit frame where $t = -\mathbf{q}^2$, is then

$$\langle \mu_1 \,|\, S(k, \mathbf{q}) \,|\, M \rangle = \langle 2p\,[{}^1S_0] \,|\, \sigma^\dagger_{1\mu_1}\, e^{i\,\mathbf{q}\cdot\mathbf{s}/2} \,|\, d\,1M \rangle . \quad (13)$$

If we quantize along the momentum transfer it becomes diagonal [11],

$$\langle M|S(k,q)|M\rangle = \begin{cases} S^+(k,q) & M = 0 \quad \text{(longitudinal)} \\ S^-(k,q) & M = \pm 1 \quad \text{(transverse)} \end{cases}$$

$$= \begin{cases} \int u_k(s) j_0\left(\frac{qs}{2}\right) U(s)ds + \sqrt{2} \int u_k(s) j_2\left(\frac{qs}{2}\right) W(s)ds, & M = 0 \\ \int u_k(s) j_0\left(\frac{qs}{2}\right) U(s)ds - \frac{1}{\sqrt{2}} \int u_k(s) j_2\left(\frac{qs}{2}\right) W(s)ds, & M = \pm 1. \end{cases} \quad (14)$$

The difference between the longitudinal and transverse form factors arises from the interference between the ${}^3S_1$ and ${}^3D_1$ states of the deuteron.

It has proven possible to describe the transition in the probe by effective form factors which depend on the four-momentum transfer only,

$$|S^\pm(t)|^2 = \frac{\int_0^\infty \left(\frac{d\sigma}{dk}\right)_{\substack{\text{spec} \\ \text{coll}}} \left| \frac{S^\pm(k,t)}{S^\pm(k,t_0)} \right|^2 dk}{\int_0^\infty \left(\frac{d\sigma}{dk}\right)_{\substack{\text{spec} \\ \text{coll}}} \left| \frac{S^\pm(k,0)}{S^\pm(k,t_0)} \right|^2 dk} , \quad (15)$$

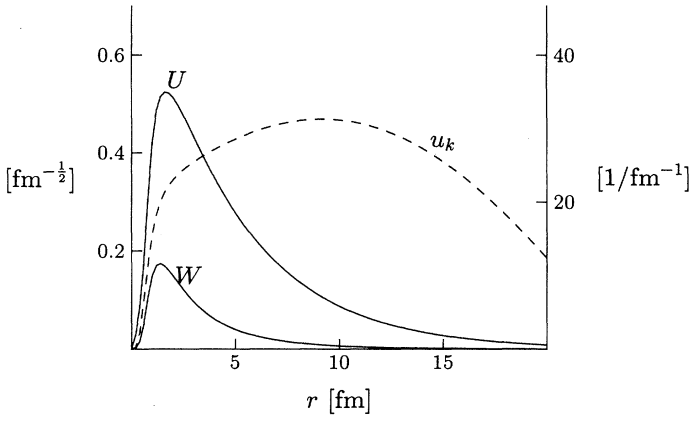

FIG. 3. Diproton $^1S_0$ wave function u_k corresponding to $k = 0.12\,\mathrm{fm}^{-1}$, dashed curve, units on the right axis. Paris parametrization of the deuteron $^3S_1$ and $^3D_1$ wave functions, units on the left axis.

with $t_0 = -1\,\mathrm{fm}^{-2}$. Here the typical theoretical k distribution, represented by $|S^{\pm}(k,t_0)|^2$, is divided out and replaced by the experimentally allowed distribution as calculated taking into account the cuts from the collimator and the spectrograph SPES4 shown in Fig. 2. The choice $t_0 = -1\,\mathrm{fm}^{-2}$ has been checked not to be crucial: the detailed k dependence of the form factors is not important. Finally, the form factor is normalized to unity at $t = 0\,\mathrm{fm}^{-2}$.

The form factors may, when $\sqrt{-t} < 2.4$ fm^{-1}, be parametrized as

$$S^-(t) = 1.31\,\exp(-1.38\,\mathrm{fm}\,\sqrt{-t}) - 0.31\,\exp(-7.30\,\mathrm{fm}\,\sqrt{-t}), \tag{16}$$

$$S^+(t) = S^-(t)\,\exp(-0.13\,\mathrm{fm}^2\,t), \tag{17}$$

$$F(t) = \left|\frac{S^+(t)}{S^-(t)}\right|^2 = \exp(-0.26\,\mathrm{fm}^2\,t)\ . \tag{18}$$

The ratio $F(t)$ expresses the emphasis the $(d,{}^2\mathrm{He})$ probe puts on the longitudinal channel. At typical values of the four-momentum transfer it can be of appreciable magnitude, for example $F(-4\,\mathrm{fm}^{-2}) = 2.8$. Thus the unpolarized cross section can be dominantly longitudinal even when the nucleon-nucleon interaction is predominantly transverse.

If we choose $k = 0.12\,\mathrm{fm}^{-1}$, the form factors $S^{\pm}(k,t)$ are, apart from normalization, almost identical to the effective form factor (15). In this sense the choice $k = 0.12\,\mathrm{fm}^{-1}$, corresponding to an excitation energy of the diproton of $E_{2p} = 0.6\,\mathrm{MeV}$, represents the average value of the relative momentum of the two ejectile protons for the experimental setup used in the results presented here. In the calculations including absorption it has been checked that the absorption does not change the k distribution: The absorption is effectively independent of k for the range of k of interest here.

C. Efficiency correction

The integral over the relative momentum k of the two protons in (15) is done once and for all, using a typical experimental distribution of k as represented by the calculated curve in Fig. 2. In doing so, we have neglected the $|\mathbf{p}_{2p}|$ dependence of the experimental cuts from the spectrograph: as the momentum of the diproton decreases, the cuts from the spectrograph become narrower. The cuts scale like $|\mathbf{p}_{2p}|$ for each of the three dimensions of $\mathbf{k}$. In all, this calls for a geometric efficiency correction $|\mathbf{p}_{2p}|^{-3}$. In the quasifree region, this correction is not very dramatic; as an example, at 1600 MeV bombarding energy it amounts to 13% at the quasielastic peak at $2.4\,\mathrm{fm}^{-1}$ momentum transfer.

The correction comes on top of the efficiency correction within the 7% acceptance of each momentum setting of the spectrograph. The efficiency, within the 7% momentum acceptance of the spectrograph, was measured by stepping the central spectrograph momentum around the elastic peak value in the $p(d,2p)n$ reaction, keeping the scattering angle fixed.

Both corrections have been done in all shown spectra. By performing the integral over final state phase space with the cuts from spectrometer and collimator imposed on the integration region, averaging over initial momenta as emitted by the synchrotron, $|\mathbf{p}_{2p}|^{-3}$-correcting the result, and then comparing with the effective form factor result, the efficiency correction procedures have proven valid on the 2% level. The polarization response is formed as a ratio of cross sections and is insensitive to these procedures.

D. Reference targets

The proton and deuteron targets serve as reference targets. In the plane wave impulse approximation (PWIA) the cross section is expressed

$$\frac{d\sigma}{dt} = \frac{1}{3}\left(\frac{m_d}{m_N}\right)^2 \frac{4}{64\,\pi\,F^2} \times \left\{(|\beta|^2 + |\varepsilon|^2 + |\gamma|^2)\,|S^-(t)|^2 + |\delta|^2\,|S^+(t)|^2\right\}, \tag{19}$$

in terms of the nucleon-nucleon isospin amplitudes [12]. $F = |\mathbf{p}_{\mathrm{lab}}|\,m_N$ is the incoming flux. The spin-longitudinal amplitude δ is multiplied by the spin-

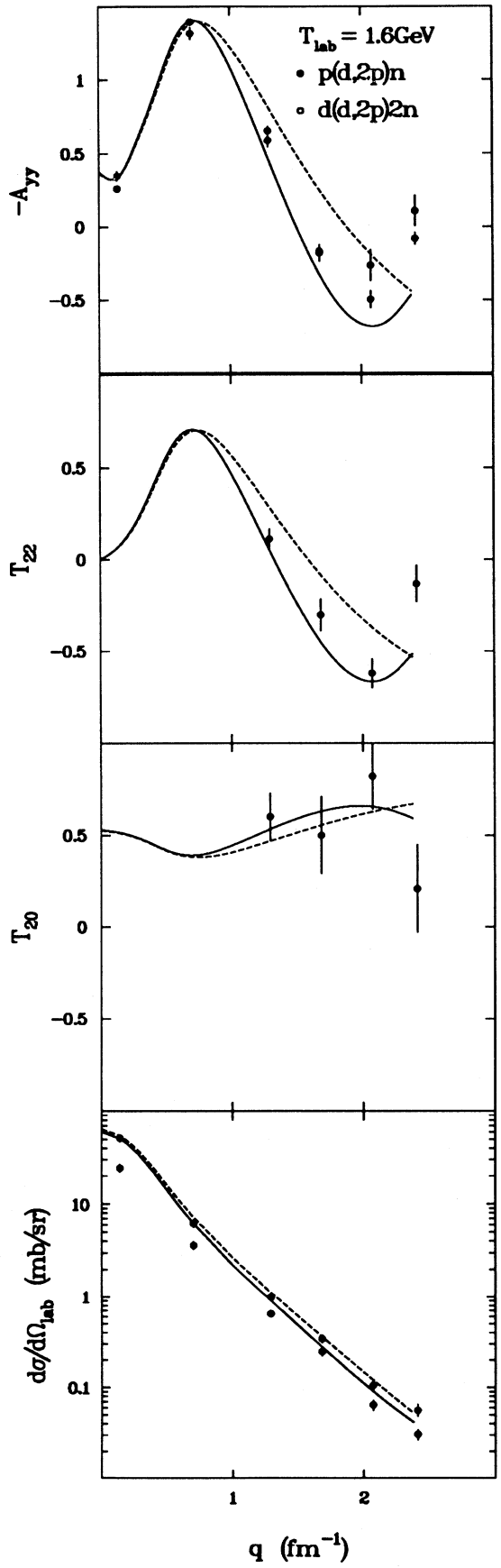

longitudinal form factor. The spin-transverse amplitudes β and ε, and the spin-orbit amplitude γ are multiplied by the spin-transverse form factor. [See Eqs. (29) and (30) for a definition of the amplitudes.]

In Fig. 4 the measured angular distributions on proton and deuteron targets are shown. The distribution predicted in the plane wave approximation is seen to reproduce very well the data all the way out to momentum transfer of 2.4 fm^{-1}.

In PWIA, the tensor analyzing powers are given by

$$T_{20}^M = \frac{1}{\sqrt{2}} \frac{|\gamma|^2 + |\beta|^2 + |\delta|^2 F(t) - 2|\varepsilon|^2}{|\beta|^2 + |\varepsilon|^2 + |\gamma|^2 + |\delta|^2 F(t)}, \tag{20}$$

$$T_{22}^M = \frac{\sqrt{3}}{2} \frac{|\beta|^2 + |\gamma|^2 - |\delta|^2 F(t)}{|\beta|^2 + |\varepsilon|^2 + |\gamma|^2 + |\delta|^2 F(t)}. \tag{21}$$

Since, phenomenologically, the transverse amplitude ε and the spin-orbit amplitude γ are small, at the bombarding energy in question, T_{22} gives a quite good separation between the spin-longitudinal δ and the spin-transverse β. The simple picture is that T_{22} is large positive for a transverse reaction mechanism, and large negative for a spin longitudinal reaction. T_{20} will be close to the maximal value, and is not sensitive to relative changes between the spin-longitudinal δ and the spin-transverse ε. At two scattering angles, we have only measured A_{yy}. However, $-A_{yy}$, being the weighted sum (8) of T_{22} and T_{20}, is almost as sensitive to the balance between spin-longitudinal and spin-transverse cross sections as is T_{22}.

In Fig. 4 the plane wave calculation is compared to the measured tensor analyzing powers. The measured polarization response is quite well described in the plane wave description at low momentum transfers. At larger momentum transfers the agreement is not so impressive. However, a Glauber calculation which includes scattering of the spectator in the spin-scalar channel gives a much improved description of the data, lending us confidence in our understanding of the probe.

Another interesting quantity to form is the ratio of cross section with unnatural-parity exchange divided by cross section with natural-parity exchange

$$R = \frac{2 + A_{yy}^M}{1 - A_{yy}^M}. \tag{22}$$

FIG. 4. The measured tensor polarization responses $-A_{yy}^{\text{lab}}$, T_{22}^M, and T_{20}^M on proton and deuteron targets are shown in the upper three panels. The dashed line is the plane wave prediction using the phenomenological nucleon-nucleon amplitudes at 800 MeV laboratory bombarding energy [36]. The solid line includes rescattering in the Glauber approach on the proton target. The measured differential cross section on proton and deuteron targets is shown in the lower panel. The proton data have been normalized to the Glauber calculation at $q = 0.7$ fm^{-1}, corresponding to 0.85 times the PW normalization. Disregarding the zero degree point where the cross section is reduced on the deuteron because of Pauli blocking of the final state, the ratio between cross section on deuteron and proton targets is 0.68 ± 0.04.

The PWIA calculation on the proton target is given by

$$R_{p(\vec{d},^2\mathrm{He})n} \overset{\mathrm{PW}}{=} \frac{|\varepsilon|^2 + |\delta|^2 F(t)}{|\gamma|^2 + |\beta|^2} . \quad (23)$$

The spin-transverse ε being small, R is very sensitive to the balance between spin-longitudinal and spin-transverse cross section. It can be independently normalized to the reference target for data and calculation. The ratio between cross section with unnatural and natural parity exchange has previously been used as a measure of collectivity in the $(\vec{p},\vec{n})$ reaction [33].

E. Distortion calculation

For the composite $(d,{}^2\mathrm{He})$ probe, the product of the incoming and outgoing distorted waves is written

$$\chi_f^\dagger(\mathbf{r}_1,\mathbf{r}_2)\,\chi_i(\mathbf{r}_1,\mathbf{r}_2) = e^{i\,\mathbf{q}_{\mathrm{ex}}\cdot(\mathbf{r}_1+\mathbf{r}_2)/2}\,D_1(b_1)\,D_2(b_2) \times\psi_{2p}^\dagger(\mathbf{r}_2-\mathbf{r}_1)\,\psi_d(\mathbf{r}_2-\mathbf{r}_1), \quad (24)$$

with distortion functions D_1 and D_2 acting on the probe nucleons separately. It is assumed that the distortion can be factorized, an approximation discussed for the $(^3\mathrm{He},t)$ reaction by Dmitriev [34]. In the eikonal limit of Glauber theory the distortion function for the spectator is

$$D_2(b) = e^{-\bar{\gamma}\,\tilde{\rho}(b)} = \exp\left(-\bar{\gamma}\int\rho[(b^2+Z^2)^{\frac{1}{2}}]\,dZ\right) . \quad (25)$$

The nuclear density distribution $\rho(r)$ is taken from electron scattering data [35]. For the particle undergoing charge exchange the nuclear thickness $\tilde{\rho}(b)$ is multiplied by $(A-1)/A$ to take into account that it has the chance of being rescattered on one target nucleon less than the spectator. At 800 MeV bombarding energy per nucleon the distortion parameter is $\bar{\gamma} = (2.1 + i\,0.3)\,\mathrm{fm}^2$ [36]; in the optical limit this corresponds to $\sigma_{NN}^{\mathrm{tot}} = 2\,\mathrm{Re}\,\bar{\gamma} = 42\,\mathrm{mb}$. The distortion functions are transformed to momentum representation

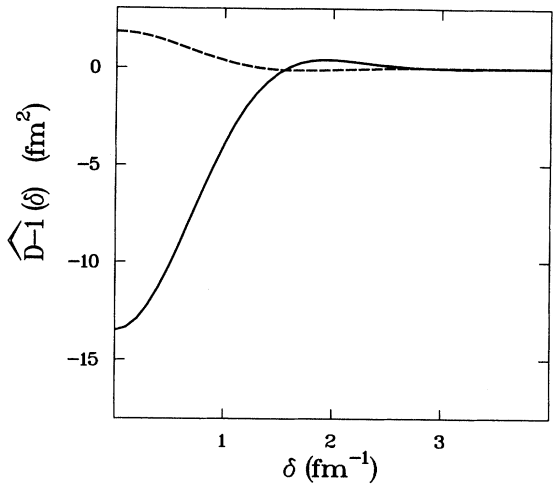

FIG. 5. Eikonal limit of the distortion function for the spectator in momentum space for the ^{12}C target at 800 MeV bombarding energy per nucleon. The dashed line is the imaginary part. When taking into account the phase space factor proportional to the distorting momentum δ, we see that the typical distorting momentum transfer is of order 1 fm^{-1}.

$$\begin{aligned} D(\boldsymbol{\delta}) &= (2\pi)^2\,\delta^{(2)}(\boldsymbol{\delta}) + \widehat{D-1}(\delta) \\ &= (2\pi)^2\,\delta^{(2)}(\boldsymbol{\delta}) + \int d^2b\,e^{i\boldsymbol{\delta}\cdot\mathbf{b}}\,(D(b)-1) \\ &= (2\pi)^2\,\delta^{(2)}(\boldsymbol{\delta}) + 2\pi\int J_0(\delta\,b)\,(D(b)-1)\,b\,db, \end{aligned} \quad (26)$$

where the distorting momentum transfer $\boldsymbol{\delta} = \mathbf{q}_{\mathrm{ex}}-\mathbf{q}$ is perpendicular to the probe momentum. The range of $\widehat{D-1}$ is inversely proportional to the nuclear radius; for ^{12}C it is of order 1 fm^{-1}. The distortion function for the ^{12}C target at 800 MeV is shown in Fig. 5.

With the above approximations the scattering matrix reads

$$\mathcal{M} = \sqrt{2}\,\frac{m_1 m_2}{m_N m_N}\,i\sum_{\mu_1\sigma_2\mu_2}\int\frac{d^2\delta}{(2\pi)^2}\langle\,\mu_1\,|\,f(\mathbf{q}_{\mathrm{ex}},\boldsymbol{\delta})\,|\,M\,\rangle\;t_{1\mu_1\,\sigma_2\mu_2}(\mathbf{q}_{\mathrm{ex}}-\boldsymbol{\delta})\,\langle\,n\,|\,\hat{j}^\dagger_{1-1\;\sigma_2\mu_2}(\mathbf{q}_{\mathrm{ex}}-\delta)\,|\,\hat{0}\,\rangle\;. \quad (27)$$

This is an integral over distorting momentum transfer of the product of the probe weight function f, the driving force t, and the target form factor $i\,\langle\,n\,|\,\hat{j}^\dagger(\mathbf{q})\,|\,\hat{0}\,\rangle$.

The probe weight function $f(\mathbf{q}_{\mathrm{ex}},\boldsymbol{\delta})$ in (27) is

$$\begin{aligned} \langle\,\mu_1\,|\,f(\mathbf{q}_{\mathrm{ex}},\boldsymbol{\delta})\,|\,M\,\rangle &= (2\pi)^2\delta^{(2)}(\boldsymbol{\delta})\,\langle\,\mu_1\,|\,S(\mathbf{q}_{\mathrm{ex}})\,|\,\rangle + \widehat{D_1-1}(\delta)\,\langle\,\mu_1\,|\,S(\mathbf{q}_{\mathrm{ex}})\,|\,M\,\rangle + \widehat{D_2-1}(\delta)\,\langle\,\mu_1\,|\,S(\mathbf{q}_{\mathrm{ex}}-2\boldsymbol{\delta})\,|\,M\,\rangle \\ &\quad + \int\frac{d^2\delta_2}{(2\pi)^2}\,\widehat{D_1-1}(|\boldsymbol{\delta}-\boldsymbol{\delta}_2|)\,\widehat{D_2-1}(\delta_2)\,\langle\,\mu_1\,|\,S(\mathbf{q}_{\mathrm{ex}}-2\boldsymbol{\delta}_2)\,|\,M\,\rangle\;. \end{aligned} \quad (28)$$

The first term is the plane wave contribution. The second term represents rescattering of the reacting nucleon, and is symmetric around the probe momentum. The third term is a term where the spectator is rescattered. The fourth term represents rescattering of both projectile nucleons. The terms with rescattering of only one probe nucleon are predominantly interfering destructively with the plane wave term, the term where both projectile nucleons are rescattered is interfering constructively. The terms involving rescattering of the spectator are asymmetric: they are large when the momentum transfer is shared by the two probe nucleons. There is a delicate

competition between the three rescattering terms and the plane wave term. In all four terms of (28), the difference between the momentum transfer on the particle undergoing charge exchange and the momentum transfer on the spectator enters in the $(d, {}^2\mathrm{He})$ form factor $S(\mathbf{q})$.

The driving force is resolved in spherical tensor components, the rank $\sigma = 0, 1$ and the component $\mu = -\sigma, ..., \sigma$ of the interaction is specified at both vertices.[2] In a coordinate system with axes defined by the CM momenta along $-\mathbf{q} = \mathbf{k}_f - \mathbf{k}_i$, $\mathbf{k}_i \times \mathbf{k}_f$ and $\mathbf{k}_i + \mathbf{k}_f$ it reads

$$\begin{aligned}\langle pn \,|\, t^{\mathrm{CM}}(\mathbf{q})\, \boldsymbol{\tau}^1 \cdot \boldsymbol{\tau}^2 \,|\, np \rangle \\ &= 2\,[\alpha + \beta\, \sigma_y^1\, \sigma_y^2 - i\,\gamma\,(\sigma_y^1 + \sigma_y^2) + \delta\, \sigma_x^1\, \sigma_x^2 + \varepsilon\, \sigma_z^1\, \sigma_z^2] \\ &= \sum_{\substack{\sigma_1 \mu_1 \\ \sigma_2 \mu_2}} t^{\mathrm{CM}}_{\sigma_1 \mu_1\, \sigma_2 \mu_2}(\mathbf{q})\; \sigma^\dagger_{\sigma_1 \mu_1}\; \sigma^\dagger_{\sigma_2 \mu_2}\ . \end{aligned} \tag{29}$$

Only the isospin-transfer channel contributes. In the calculation the phenomenological on-shell amplitudes of Bugg were used [36,37]. The normalization is

$$\frac{d\sigma}{dt}(np \to pn) = \frac{4}{64\pi F^2} \sum_{\substack{\sigma_1 \mu_1 \\ \sigma_2 \mu_2}} |t^{\mathrm{CM}}_{\sigma_1 \mu_1\, \sigma_2 \mu_2}(\mathbf{q})|^2 \tag{30}$$

with incoming flux $F = [(k_1 k_2)^2 - m_N^4]^{\frac{1}{2}}$.

The transformation from the nucleon-nucleon CM system with y axis along $\mathbf{k}_i \times \mathbf{k}_f$ to the laboratory frame with y axis along $\mathbf{p}_1 \times \mathbf{p}_3$ is to a good approximation a rotation $\psi_q = \varphi_q - \varphi_{q_{\mathrm{ex}}} = \varphi_q - \pi$ around the z axis along the laboratory probe momentum

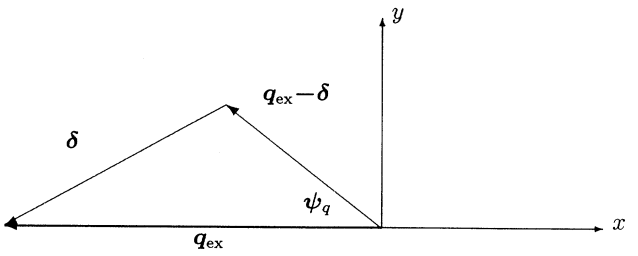

FIG. 6. The total momentum transfer $\mathbf{q}$ is shared between distortion $\boldsymbol{\delta}$ and charge exchange $\mathbf{q} = \mathbf{q}_{\mathrm{ex}} - \boldsymbol{\delta}$. Thus the direction of the underlying charge exchange is altered in direction and magnitude. As discussed in the text, the magnitude of the distorting momentum transfer is of the order $1\,\mathrm{fm}^{-1}$.

$$t_{\sigma_1 \mu_1\, \sigma_2 \mu_2}(\mathbf{q}) = e^{i\,\psi_q\,(\mu_1 + \mu_2)}\, t^{\mathrm{CM}}_{\sigma_1 \mu_1\, \sigma_2 \mu_2}(\mathbf{q})\ . \tag{31}$$

The distorting momentum transfer is of order $1\,\mathrm{fm}^{-1}$. Thus, as illustrated in Fig. 6, the rotation angle can be large. Since the amplitudes $t^{\mathrm{CM}}_{1\pm 1\, 1\pm 1} = \frac{1}{2}(\delta - \beta)$ which have $|\mu_1 + \mu_2| = 2$ dominate in the region where the spin-longitudinal is attractive, the effect of the rotation is large. The approximation (31) assumes that the momentum transfer along Z is much smaller than the perpendicular component.

The nuclear spin-isospin response function was calculated in the continuum RPA framework described in [3]. It is defined as

$$R^{\tau' \upsilon'\ \sigma' \mu'}_{\tau \upsilon\ \sigma \mu}(\mathbf{q}, \mathbf{q}', \omega) = \sum_{n \neq \hat{0}} \langle \hat{0} \,|\, \hat{j}_{\tau \upsilon\, \sigma \mu}(\mathbf{q}) \,|\, n \rangle \delta(\omega - (E_n - E_0))\, \langle n \,|\, \hat{j}^\dagger_{\tau' \upsilon'\, \sigma' \mu'}(\mathbf{q}') \,|\, \hat{0} \rangle \tag{32}$$

with the spin-isospin current

$$\hat{j}_{\tau \upsilon\, \sigma \mu}(\mathbf{q}) = i \sum_{j=1}^{A} \tau^j_{\tau \upsilon}\, \sigma^j_{\sigma \mu}\, e^{-i\,\mathbf{q} \cdot \mathbf{r}_j}\ . \tag{33}$$

The nuclear states $|\, n \,\rangle$ are eigenstates of the Hamiltonian

$$H = H_{\mathrm{sp}} + V \tag{34}$$

including the residual interaction V. If the particle-hole interaction V is turned off, the response is referred to as uncorrelated. The effective particle-hole interaction was parametrized as

$$V(\mathbf{q}, \omega) = \left(\frac{f_\pi}{m_\pi}\right)^2 \boldsymbol{\tau}^1 \cdot \boldsymbol{\tau}^2 \left[\left(g' - \frac{\mathbf{q}^2}{m_\pi^2 - t} \Gamma_\pi^2(t) \right) (\boldsymbol{\sigma}^1 \cdot \hat{\mathbf{q}})(\boldsymbol{\sigma}^2 \cdot \hat{\mathbf{q}}) + \left(g' - C_\rho \frac{\mathbf{q}^2}{m_\rho^2 - t} \Gamma_\rho^2(t) \right) (\boldsymbol{\sigma}^1 \times \hat{\mathbf{q}}) \cdot (\boldsymbol{\sigma}^2 \times \hat{\mathbf{q}}) \right] \tag{35}$$

with $m_\pi = 139\,\mathrm{MeV}$, $m_\rho = 770\,\mathrm{MeV}$, $C_\rho = 2.18$, and $f_\pi = 1.008$. Cut-off masses in the monopole form factors Γ_π and Γ_ρ were 1300 MeV and 2000 MeV, respectively [2,3]. The Landau-Migdal parameter g' was set to 0.6. Coupling to the $\Delta\,(1232\,\mathrm{MeV})$ with coupling constant $f_\pi^* = 2.0 f_\pi$ was included in the calculation. In the calculations, the universality ansatz $g'_{NN} = g'_{N\Delta} = g'_{\Delta\Delta}$ was assumed. The coupling to the Δ enhances the spin-longitudinal cross section. The validity of the universality is a current issue of debate [38].

Finally, in order to calculate the cross section (2) and polarization response (3) in the $(\vec{d}, {}^2\mathrm{He})$ reaction, we need the traces

[2]Here $\sigma_{00} = 1$, $\sigma_{10} = \sigma_z$, $\sigma_{1\pm 1} = \mp(\sigma_x \pm i\,\sigma_y)/\sqrt{2}$.

$$\mathrm{tr}(\mathcal{M}\,\tau_{\lambda\mu}\,\mathcal{M}^\dagger) = 2\left(\frac{m_1 m_2}{m_N m_N}\right)^2 \sum_{MM'} \langle 1M' \,|\, \tau_{\lambda\mu} \,|\, 1M \rangle \sum_{\substack{\mu_1\sigma_2\mu_2 \\ \mu_1'\sigma_2'\mu_2'}} \int \frac{d^2\delta}{(2\pi)^2} \int \frac{d^2\delta'}{(2\pi)^2} R^{1-1\,\sigma_2'\mu_2'}_{1-1\,\sigma_2\mu_2}(\mathbf{q}_{\mathrm{ex}}-\boldsymbol{\delta}, \mathbf{q}_{\mathrm{ex}}-\boldsymbol{\delta}', \omega)$$
$$\times \langle \mu_1 \,|\, f(\mathbf{q}_{\mathrm{ex}}, \boldsymbol{\delta}) \,|\, M \rangle^* \; t^*_{1\mu_1\,\sigma_2\mu_2}(\mathbf{q}_{\mathrm{ex}}-\boldsymbol{\delta}) \; \langle \mu_1' \,|\, f(\mathbf{q}_{\mathrm{ex}}, \boldsymbol{\delta}') \,|\, M' \rangle \; t_{1\mu_1'\,\sigma_2'\mu_2'}(\mathbf{q}_{\mathrm{ex}}-\boldsymbol{\delta}') \; . \qquad (36)$$

IV. RESULTS AND DISCUSSION

The results of the measurements on the ^{12}C target are shown in Figs. 7–14, as are results of the above calculation.

Looking first at the cross section data, the position of the quasielastic peak follows a dispersion relation different from that on a free nucleon given in Eq. (1) and indicated by the arrow in the figures. The observed peak position corresponds qualitatively to distributing the available momentum transfer on two target nucleons. Neither the PWIA nor the DWIA calculation shows a significant effect of correlations for the position of the peak. In the calculation, the spin-longitudinal component is moved downwards in energy transfer relative to the spin-transverse one, which is moved a bit upwards. But the total cross section remains practically unchanged both in magnitude and position. Particle-hole correlations do not help us in trying to understand the downward shift of the quasielastic peak at large momentum transfers.

At energy transfers larger than the Fermi energy, only part of the observed cross section is reproduced by the DWIA calculation. We take this as an indication that part of the observed cross section in the upper end of the quasielastic peak could come from higher order processes.

Now turning to the polarization responses: In the plane wave limit, the measured quantity T_{22} gives a rather good separation between spin-longitudinal and spin-transverse responses [26,10–12]: Pure spin-longitudinal cross section has negative T_{22} and spin-transverse has positive T_{22}.

For scattering angles 2.7° and 9.3° only A_{yy} was measured. Since T_{20} is insensitive to the ratio of longitudinal to transverse cross section, and A_{yy} is the weighted sum (8) of T_{22} and T_{20}, A_{yy} is equally sensitive to correlations as T_{22}.

At momentum transfer $q = 0.7\,\mathrm{fm}^{-1}$ (2.7°), shown in Fig. 7, we observe a large polarization response ($-A_{yy}$). This is consistent with the spin-longitudinal amplitude in the driving force having a zero crossing at this momentum transfer.

The plane wave calculation in Figs. 8–11 demonstrates how correlations lead to a softening and enhancement of the longitudinal response versus a hardening and quenching of the transverse response, i.e., a preference for longitudinal response in the lower end of the quasielastic peak. The tensor analyzing power T_{22} becomes an increasing function of the energy transfer over the quasifree region.

At the smallest scattering angles, 2.7° and 5.0°, the polarization response at the peak of the quasielastic bump is in fair agreement with the free response represented by the deuteron target in Fig. 4, though with a slight

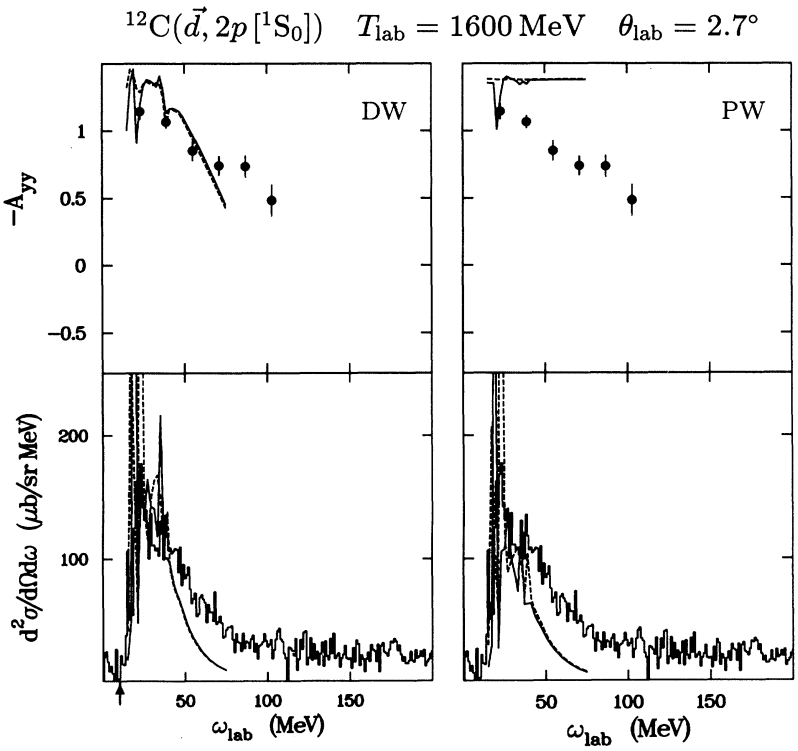

FIG. 7. Cross section and tensor polarization response in ^{12}C($\vec{d}$, 2p[$^1S_0$]) at bombarding energy 1600 MeV and 2.7° scattering angle. The momentum transfer is around $0.7\,\mathrm{fm}^{-1}$. The arrow indicates the position of the free response, i.e., the response on a proton target. The curves on the right plot are PW RPA (full) and PW uncorrelated (dash), the calculated PW cross sections have been divided by 4. The curves on the left plot are DW RPA (full) and DW uncorrelated (dash). At such a small scattering angle, the large aperture causes a significant spread in the angle of the scattering plane. Thus, expressing the analyzing power in the laboratory in terms of those in the Madison frame, the measured quantity is $A_{YY}^{\mathrm{lab}} = 0.95A_{YY}^M + 0.05A_{XX}^M = -\sqrt{2}(\frac{1}{2}\,T_{20}^M + \sqrt{\frac{3}{2}}\,0.90\,T_{22}^M)$.

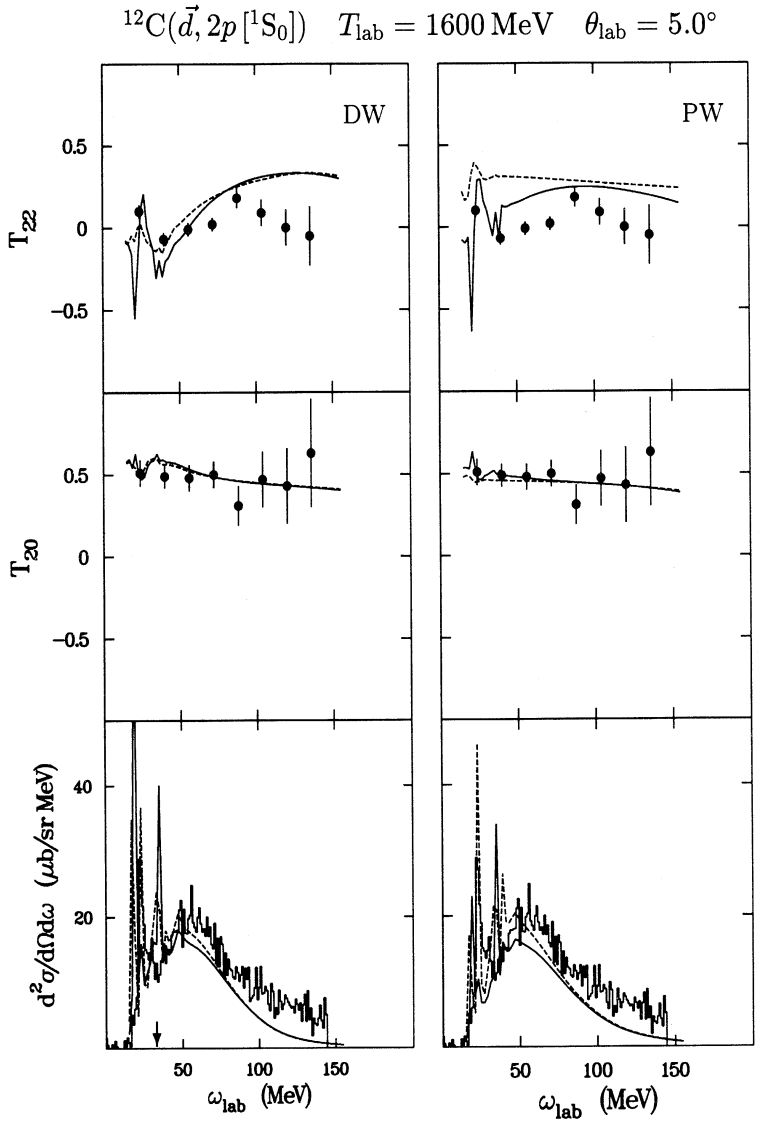

FIG. 8. Cross section and tensor polarization response at 5.0° scattering angle. The momentum transfer is around 1.3 fm^{-1}. The arrow indicates the position of the free response, i.e., the response on a proton target. The curves on the right plot are PW RPA (full) and PW uncorrelated (dash), the calculated PW cross sections have been divided by 4. The curves on the left plot are DW RPA (full) and DW uncorrelated (dash).

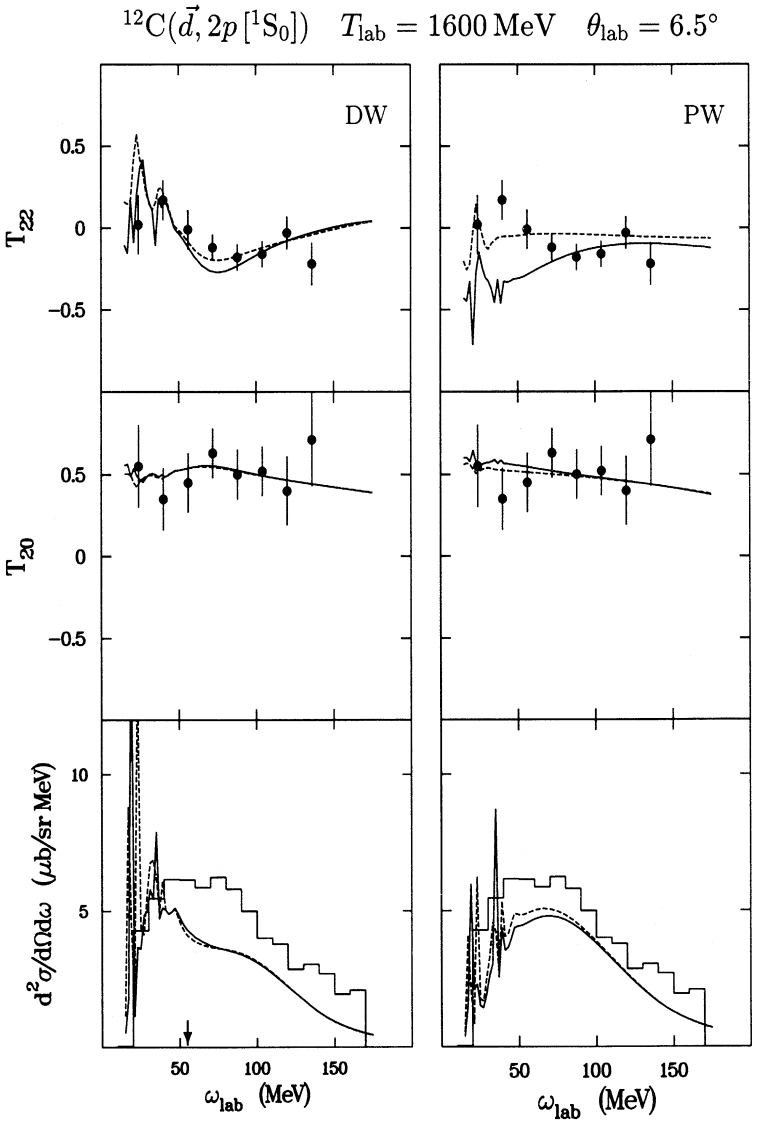

FIG. 9. As in Fig. 8, but at 6.5° scattering angle where the momentum transfer is around 1.7 fm^{-1}.

tendency towards more longitudinal response. At larger scattering angles, the measured cross section is systematically much more spin transverse than on the deuteron target. An enhancement, though smaller, of the spin-transverse over the spin-longitudinal cross section in nuclei is observed by Carey *et al.* with the $(\vec{p},\vec{p}\,')$ reaction [16,15] at momentum transfer $1.7\,\mathrm{fm}^{-1}$, and more recently by Taddeucci *et al.* in $(\vec{p},\vec{n})$ [18,19] at momentum transfers $1.7\,\mathrm{fm}^{-1}$ and $2.5\,\mathrm{fm}^{-1}$. In the latter experiment a slight enhancement of the spin-longitudinal over transverse is observed at the quasifree peak at $q = 1.2\,\mathrm{fm}^{-1}$. Despite the qualitative similarity between the results with the composite probe $(\vec{d},{}^2\mathrm{He})$ and the elementary probes, $(\vec{p},\vec{n})$ and $(\vec{p},\vec{p}\,')$, the explanation could be quite different.

Turning to the DW calculation. Here two effects come into play: First, and most important, the distortion mixes the spin-longitudinal and spin-transverse channel. Second, due to the fact that the reaction is somewhat surface peaked, thus selecting low densities, the effect of nuclear correlations is damped. Both effects damp the difference between correlated and uncorrelated response at the level of the observed quantity. In Figs. 7–11 we see that, in the continuum region, there is only little difference between the correlated and the uncorrelated polarization response.

A striking effect of distortion on T_{22} is the change of slope of the response over the quasielastic peak. Let us for a moment ignore the rotation of reference frame (31) and turn off all amplitudes but one, in the driving force. The ω dependence of the absorption factor is rather different for the individual amplitudes: At small ω the response function prefers the smaller effective momentum transfers; at large ω the response function prefers the larger effective momentum transfers. The absorption is due to the interference between the plane wave and rescattering terms, where the plane wave is evaluated at q_{ex} and rescattering is preferably evaluated at $q < q_{\mathrm{ex}}$ for

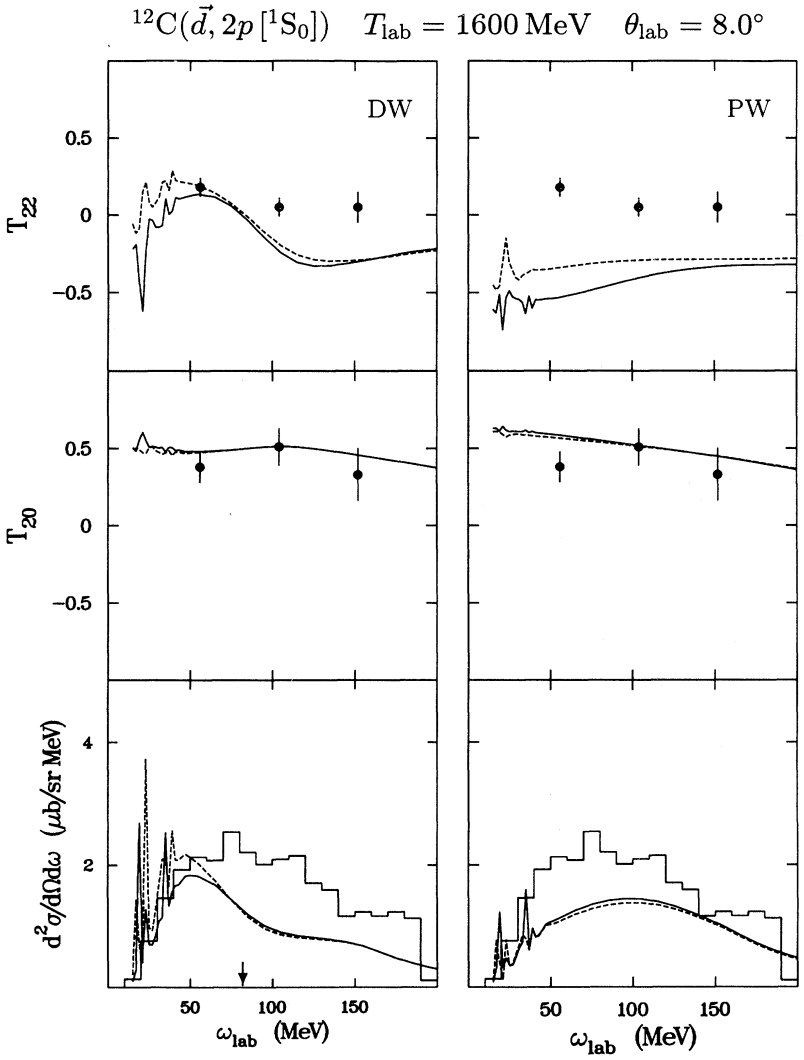

FIG. 10. As in Fig. 8, but at 8.0° scattering angle where the momentum transfer is around $2.1\,\mathrm{fm}^{-1}$.

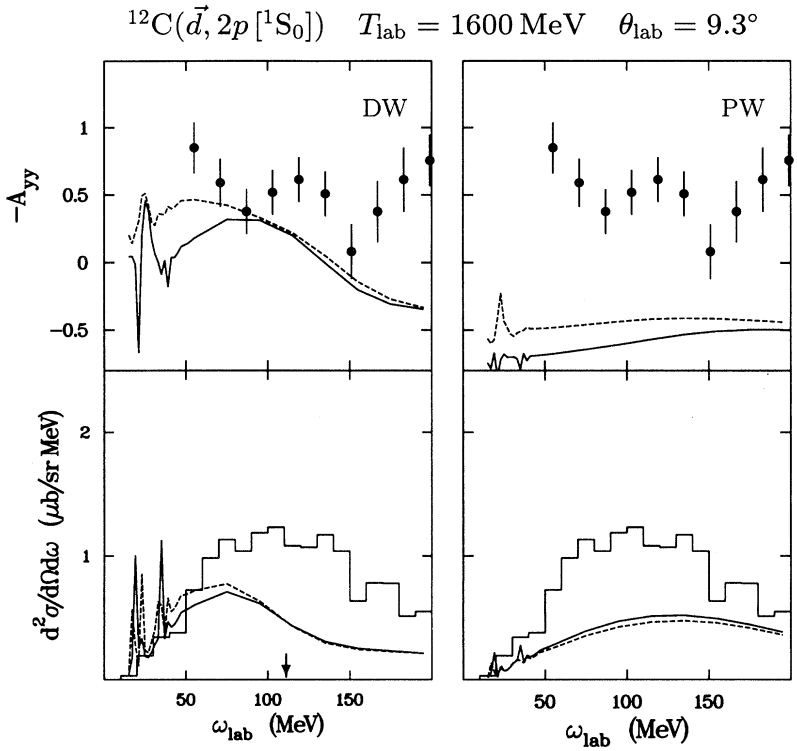

FIG. 11. As in Fig. 8, but at 9.3° scattering angle where the momentum transfer is around 2.4 fm^{-1}. The measured quantity here is $A_{YY}^M = -\sqrt{2}\left(\frac{1}{2}T_{20}^M + \sqrt{\frac{3}{2}}\,T_{22}^M\right)$.

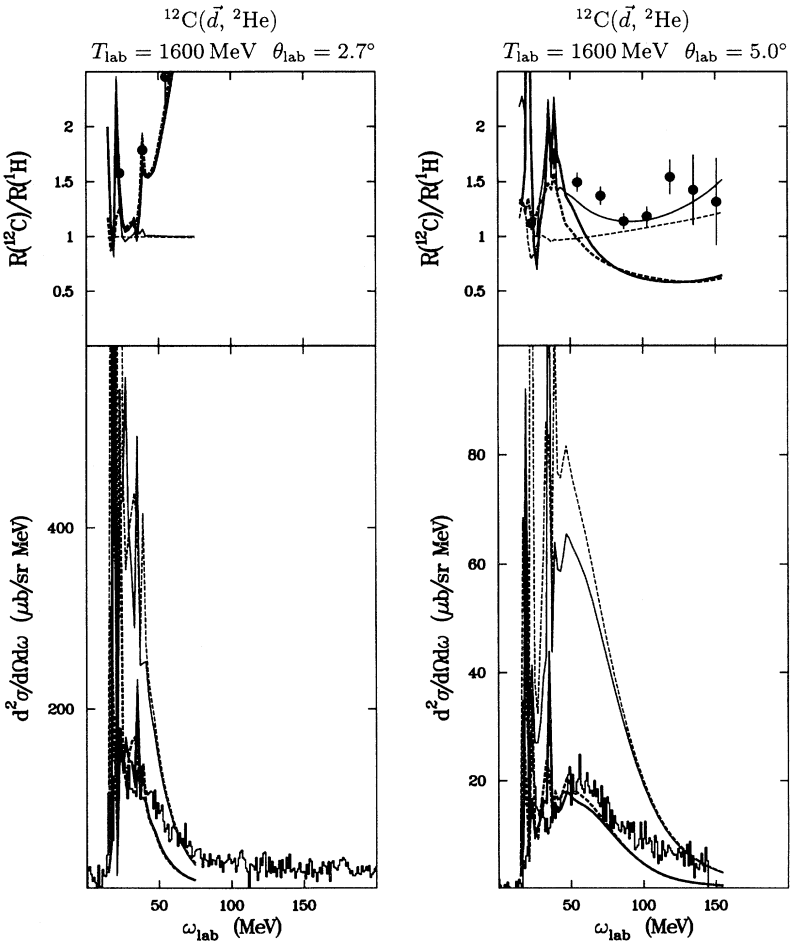

FIG. 12. Top left: The ratio of unnatural to natural parity exchange at 2.7° scattering angle normalized to the result on the ^{1}H target. The momentum transfer is around 0.7 fm^{-1}. Note, that at this momentum transfer the zero crossing of the spin-longitudinal driving interaction makes R inappropriate as a measure of spin-longitudinal collectivity. This angle is thus shown mainly for completeness. Thin curves are plane wave calculations, thick curves include distortion. Solid curves are with correlations, dashed curves are uncorrelated. Plane wave calculations are normalized to the plane wave calculation on the proton target. Distorted wave calculations are normalized to the Glauber calculation on the proton target. Bottom left: Differential cross section at 2.7°. The position of the calculated response, has been shifted 5 MeV to reproduce the position of the $J^\pi = 4^-$ state at $\omega = 18$ MeV. Top right: The ratio of unnatural to natural parity exchange at 5.0° scattering angle normalized to the result on the ^{1}H target. The momentum transfer is around 1.3 fm^{-1}. Bottom right: Differential cross section at 5.0°.

the smaller ω and at $q > q_{ex}$ for the larger ω. The absorption factor therefore becomes an increasing function of ω for amplitudes whose magnitude is a decreasing function of q and vice versa. This explains that the slope of T_{22} appears already in the cross-section-weighted sum of the polarization response for the individual amplitudes.

The mixing of the spin-longitudinal and spin-transverse channels through the rotation (31) from the nucleon-nucleon CM frame to the external frame and the interference effects between amplitudes affect the magnitude of the polarization response, but have little effect on the slope. Furthermore, it reduces the difference between the correlated and uncorrelated response.

We saw, in the discussion on the elastic distortion, that the rescattering distributes the momentum transfer on the two probe nucleons. This is also intuitively clear, since the two protons are required to be in a quasibound state. The same argument applies for the case of inelastic rescattering. Thus, when the energy transfer is so high that the final state Pauli blocking is not important, inelastic rescattering may carry a large component of the cross section. At smaller energy transfer the two-step inelastic process is highly blocked and its cross section is expected to describe only a minor fraction of the observed. This may explain why the distortion calculation, which only accounts for rescattering in the elastic channel, underestimates the cross section at large energy transfers, and may further explain that the quasielastic peak is shifted down in energy transfer at large momentum transfers.

In Figs. 12–14 the results are shown as the ratio between the cross section with unnatural-parity exchange and the cross section with natural-parity exchange given in Eq. (22). In order to minimize uncertainties from the elementary charge-exchange amplitudes used in the calculation, the ratio is normalized to the result on the proton target for the data and the calculation independently.

Let us take a look at Fig. 13 where the result obtained with the $(\vec{d},{}^2\mathrm{He})$ probe is compared with that obtained in $(\vec{p},\vec{n})$ at LAMPF [18]. From the PWIA calculations (thin curves) we see that the suggested ratio is indeed sensitive to correlations: the ratio of unnatural over natural parity exchange is enhanced in the lower end of the quasifree peak. In the DWIA calculations, we see that the sensitivity to correlations survives in the (p,n) reac-

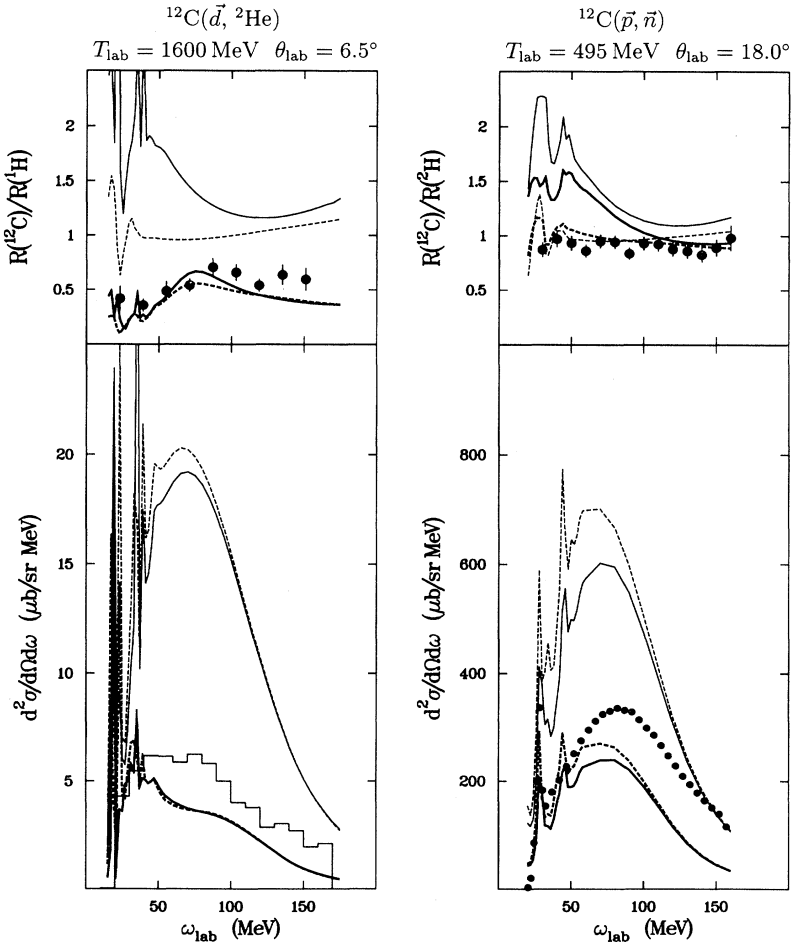

FIG. 13. Top left: The ratio of unnatural to natural parity exchange in $^{12}C(\vec{d},{}^2He)$ at bombarding energy 1600 MeV and 6.5° scattering angle normalized to the result on the ^1H target. The momentum transfer is around 1.7 fm^{-1}. Thin curves are plane wave calculations, thick curves include distortion. Solid curves are with correlations, dashed curves are uncorrelated. Plane wave calculations are normalized to the plane wave calculation on the proton target. Distorted wave calculations are normalized to the Glauber calculation on the proton target. Bottom left: Differential cross section in $^{12}C(d,{}^2He)$ at 6.5°. The position of the calculated response has been shifted 5 MeV to reproduce the position of the $J^\pi = 4^-$ state in ^{12}B at $\omega = 18$ MeV. Top right: The ratio of unnatural to natural parity exchange in $^{12}C(\vec{p},\vec{n})$ at bombarding energy 495 MeV and 18° scattering angle normalized to the result on the ^2H target. The momentum transfer is around 1.7 fm^{-1}. Thin curves are plane wave calculations, thick curves include distortion. Full curves are with correlations, dashed curves are uncorrelated. The data points are from Ref. [17] and the calculation from Ref. [33]. Bottom right: Differential cross section in $^{12}C(p,n)$ at 18°. The calculations were shifted 10 MeV to reproduce the position of the 4^- state in ^{12}N.

tion, whereas in $(d, {}^2\mathrm{He})$ the sensitivity to RPA correlations is destroyed resulting in practically identical results for correlated and uncorrelated ratios. We note that in $(\vec{p}, \vec{n})$ only the uncorrelated calculation shows agreement with data.

At larger momentum transfers shown in Fig. 14 the picture is similar. The experimentally observed differential cross section is only accounted for at small energy transfers. In the PWIA the ratio R between unnatural and natural-parity exchange is sensitive to RPA correlations. Distortion brings the correlated as well as the uncorrelated calculated ratio in qualitative agreement with data.

At $q = 1.3\,\mathrm{fm}^{-1}$ $(5.0°)$ shown in Fig. 12 the observed ratio indicates an enhancement of R. Since also the RPA calculation shows an enhancement of R in the lower end of the quasielastic peak, we could be tempted to conclude, that the predicted collectivity were to be found here. However, when we look at the DWIA calculation, we again find that the correlated and uncorrelated calculations are essentially identical, and both in qualitative agreement with data.

The smallest momentum transfer $q = 0.7\,\mathrm{fm}^{-1}$ $(2.7°)$, also shown in Fig. 12, is shown mainly for completeness. Here the spin-longitudinal driving force vanishes. Thus R measures the ratio between the transverse along the beam and the transverse perpendicular to the scattering plane [see Eq. (22)].

V. CONCLUSION

Experimental data on the nuclear spin-isospin response in the quasifree region, measured with the charge-exchange reaction $(\vec{d}, 2p[{}^1S_0])$ at Laboratoire National Saturne, have been presented.

A careful analysis of the whole process including distortion of the two projectile nucleons has been made in the eikonal limit. Effects of absorption are found to be large, bringing the calculated tensor analyzing power closer to the observed. In regions where the cross section is reproduced, i.e., at small energy transfers, also the observed analyzing power is in qualitative agreement with the calculation. Distortion effects are found to seriously dilute the sensitivity to a possible medium polarization.

At larger momentum transfers the present model calculations underestimate the cross section in the high energy end of the quasielastic peak, indicating significant contri-

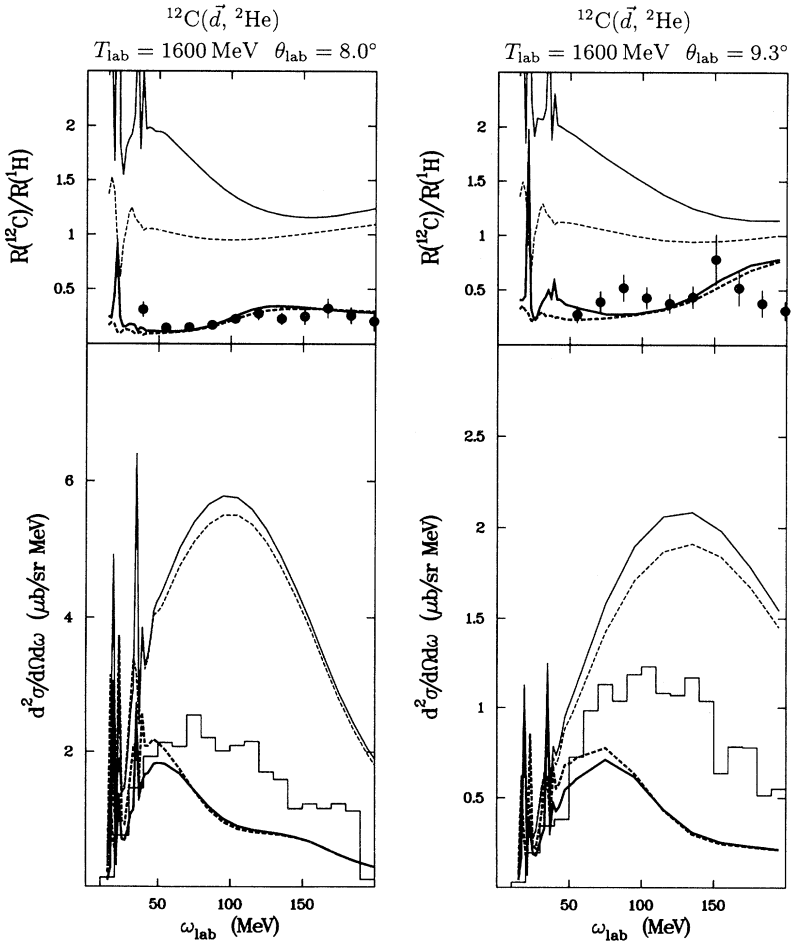

FIG. 14. Top left: The ratio of unnatural to natural parity exchange at 8.0° scattering angle normalized to the result on the ^{1}H target. The momentum transfer is around $2.1\,\mathrm{fm}^{-1}$. See Fig. 12. Bottom left: Differential cross section at 8.0°. Top right: The ratio of unnatural to natural parity exchange at 9.3° scattering angle normalized to the result on the ^{1}H target. The momentum transfer is around $2.4\,\mathrm{fm}^{-1}$. See Fig. 12. Bottom right: Differential cross section at 9.3°.

butions from higher order processes. A recent analysis of electron scattering data suggests that contributions from two-body operators in the probing field are quite large in the spin-transverse channel. Inclusion of higher order effects like two-body contributions and two-step processes together with distortion effects are, however, quite complicated for hadronic probes and awaits further theoretical progress.

ACKNOWLEDGMENTS

We gratefully acknowledge the support from the technical staff at Laboratoire National Saturne. This work has been supported in part by IN2P3 of CNRS, by the Danish and Swedish National Research Councils, and by the Carlsberg Foundation.

[1] W. M. Alberico, M. Ericson, and A. Molinari, Phys. Lett. **92B**, 153 (1980).
[2] W. M. Alberico, M. Ericson, and A. Molinari, Nucl. Phys. **A379**, 429 (1982).
[3] M. Ichimura, K. Kawahigashi, T. S. Jørgensen, and C. Gaarde, Phys. Rev. C **39**, 1446 (1989).
[4] J. Carlson and R. Schiavilla, Phys. Rev. C **49**, R2280 (1994).
[5] I. Bergqvist, A. Brockstedt, L. Carlén, P. Ekström, B. Jakobsson, C. Ellegaard, C. Gaarde, J. S. Larsen, C. Goodman, M. Bedjidian, D. Contardo, J. Y. Grossiord, A. Guichard, R. Haroutunian, J. R. Pizzi, D. Bachelier, J. L. Boyard, T. Hennino, J. C. Jourdain, M. Roy-Stephan, M. Boivin, and P. Radvanyi, Nucl. Phys. **A469**, 648 (1987).
[6] P. Barreau, M. Bernhein, J. Duclos, J. M. Finn, Z. Meziani, J. Morgenstern, J. Mougey, D. Royer, B. Saghai, D. Tarnowski, S. Turck-Chieze, M. Brussel, G. P. Capitani, E. de Sanctis, S. Frullani, F. Garibaldi, D. B. Isabelle, E. Jans, I. Sick, and P. D. Zimmerman, Nucl. Phys. **A402**, 515 (1983).
[7] C. Gaarde, Nucl. Phys. **A478**, 475c (1988).
[8] T. N. Taddeucci, in *Proceedings of the Telluride Conference on Spin and Iso-spin in Nuclear Interactions* (Plenum, New York, 1991).
[9] C. Ellegaard, C. Gaarde, T. S. Jørgensen, J. S. Larsen, B. Million, C. Goodman, A. Brockstedt, P. Ekström, M. Österlund, M. Bedjidian, D. Contardo, D. Bachelier, J. L. Boyard, T. Hennino, J. C. Jourdain, M. Roy-Stephan, P. Radvanyi, and P. Zupranski, Phys. Lett. **231B**, 365 (1989).
[10] D. V. Bugg and C. Wilkin, Phys. Lett. **152B**, 57 (1985).
[11] C. Wilkin and D. V. Bugg, Phys. Lett. **154B**, 243 (1985).
[12] D. V. Bugg and C. Wilkin, Nucl. Phys. **A467**, 575 (1987).
[13] T. Sams and V. F. Dmitriev, Phys. Rev. C **45**, R2555 (1992).
[14] T. Sams, in *RIKEN International Workshop on Delta Excitation in Nuclei*, RIKEN, Wako-shi, Japan (World Scientific, Singapore, 1994), p. 301.
[15] L. B. Rees, J. M. Moss, T. A. Carey, K. W. Jones, J. B. McClelland, N. Tanaka, A. D. Bacher, and H. Esbensen, Phys. Rev. C **34**, 627 (1986).
[16] T. Carey, J. Phys. Soc. Jpn. (Suppl.) **55**, 172 (1986).
[17] J. B. McClelland, T. N. Taddeucci, X. Y. Chen, W. P. Alford, R. C. Byrd, T. A. Carey, S. DeLucia, C. D. Goodman, E. Gülmez, W. Huang, B. Luther, D. G. Marchlenski, D. J. Mercer, D. L. Prout, J. Rapaport, L. J. Rybarcyk, W. Sailor, E. Sugarbaker, Y. Wang, and C. Whitten, Jr., Phys. Rev. Lett. **69**, 582 (1992).
[18] X. Y. Chen, T. N. Taddeucci, J. B. McClelland, T. A. Carey, R. C. Byrd, L. J. Rybarcyk, W. C. Sailor, D. J. Mercer, D. L. Prout, S. DeLucia, B. Luther, D. G. Marchlenski, E. Sugarbaker, J. Rapaport, E. Gülmez, C. A. Whitten, Jr., C. D. Goodman, W. Huang, Y. Wang, and W. P. Alford, Phys. Rev. C **47**, 2159 (1993).
[19] T. N. Taddeucci, B. A. Luther, L. J. Rybarcyk, R. C. Byrd, J. B. McClelland, D. L. Prout, S. DeLucia, D. A. Cooper, D. G. Marchlenski, E. Sugarbaker, B. K. Park, T. Sams, C. D. Goodman, and J. Rapaport, Phys. Rev. Lett. **73**, 3516 (1994).
[20] V. R. Pandharipande, J. Carlson, S. C. Pieper, R. B. Wiringa, and R. Schiavilla, Phys. Rev. C **49**, 789 (1994).
[21] T. Sams, Ph.D. thesis, Niels Bohr Institutet, Københavns Universitet, 1990.
[22] T. Sams, in *Proceedings of the Telluride Conference on Spin and Isospin in Nuclear Interactions* (Plenum, New York, 1991).
[23] P. A. Chamouard, M. Olivier, G. Rommel, and A. Tkatchenko, Bulletin Nouvelles de Saturne, DOC-CEN-SACLAY **12**, 7 (1987).
[24] J. L. Laclare, J. M. Lefebvre, P. A. Chamouard, and A. Ropert, Bulletin Nouvelles de Saturne, DOC-CEN-SACLAY **9B**, 1 (1984), *MIMAS*.
[25] E. Grorud, J. L. Laclare, A. Ropert, A. Tkatchenko, J. Banaigs, and M. Boivin, Nucl. Instrum. Meth. Phys. Res. **A188**, 549 (1981).
[26] C. Ellegaard, C. Gaarde, T. S. Jørgensen, J. S. Larsen, C. Goodman, I. Bergqvist, A. Brockstedt, P. Ekström, M. Bedjidian, D. Contardo, J. Y. Grossiord, A. Guichard, D. Bachelier, J. L. Boyard, T. Hennino, J. C. Jourdain, M. Roy-Stephan, P. Radvanyi, and J. Tinsley, Phys. Rev. Lett. **59**, 974 (1987).
[27] *Proceedings of the Third International Polarization Symposium*, edited by H. H. Barschall and W. Haberli (University of Wisconsin Press, Madison, Wisconsin, 1971), p. XXV.
[28] A. Bohr, Nucl. Phys. **10**, 486 (1959).
[29] A. Boudard, Report No. CEA-N-2386, 1984; Report No. CEA-N-2584, 1988.
[30] M. Lacombe, B. Loiseau, R. Vinh Mau, J. Côte, P. Pirés, and R. de Tourreil, Phys. Lett. **101B**, 139 (1981).
[31] R. V. Reid, Jr., Ann. Phys. (Paris) **50**, 411 (1968).
[32] M. A. Preston and R. K. Bhaduri, *Structure of the Nucleus* (Addison-Wesley, Reading, MA, 1975).
[33] T. Sams, Phys. Rev. C **48**, R2162 (1993).
[34] V. F. Dmitriev, Phys. Lett. B **226**, 219 (1989).
[35] C. W. Jager, H. de Vries, and C. de Vries, Atom. Data Nucl. Data Tables **14**, 479 (1974).
[36] D. V. Bugg, "Empirical nucleon-nucleon amplitudes at lab. bombarding energies 25–800 MeV, 1992 (private communication) see also [39].
[37] A. K. Kerman, M. McManus, and R. M. Thaler, Ann. Phys. (Paris) **8**, 551 (1959).
[38] K. Nishida and M. Ichimura, Prog. Theor. Phys. **91**, 69

(1994).
[39] R. Dubois, D. Axen, R. Keeler, M. Comyn, G. A. Ludgate, J. R. Richardson, N. M. Stewart, A. S. Clough, D. V. Bugg, and J. A. Edgington, Nucl. Phys. **A377**, 554 (1982).
[40] A. B. Wicklund, M. V. Arenton, D. S. Ayres, R. Diebold, S. L. Kramer, E. N. May, L. J. Nodulman, and J. R. Sauer, Phys. Rev. D **34**, 19 (1986).
[41] A. B. Wicklund, M. V. Arenton, D. S. Ayres, R. Diebold, E. N. May, L. J. Nodulman, J. R. Sauer, E. C. Swallow, M. M. Calkin, M. D. Corcoran, J. Hoftiezer, H. E. Miettinen, and G. S. Mutchler, Phys. Rev. D **35**, 2670 (1987).